The Pertussis Toxin S1 Subunit Is a Thermally Unstable Protein Susceptible to Degradation by the 20S Proteasome†

Abhay H. Pande,‡,§,|| David Moe,‡,§ Maneesha Jamnadas,‡,⊥ Suren A. Tatulian,§ and Ken Teter*,‡,§

Department of Molecular Biology and Microbiology and Biomolecular Science Center, University of Central Florida, 12722 Research Parkway, Orlando, Florida 32826

Received June 13, 2006; Revised Manuscript Received September 14, 2006

ABSTRACT: Pertussis toxin (PT) is an AB-type protein toxin that consists of a catalytic A subunit (PT S1) and an oligomeric, cell-binding B subunit. It belongs to a subset of AB toxins that move from the cell surface to the endoplasmic reticulum (ER) before the A chain passes into the cytosol. Toxin translocation is thought to involve A chain unfolding in the ER and the quality control mechanism of ER-associated degradation (ERAD). The absence of lysine residues in PT S1 may allow the translocated toxin to avoid ubiquitin-dependent degradation by the 26S proteasome, which is the usual fate of exported ERAD substrates. As the conformation of PT S1 appears to play an important role in toxin translocation, we used biophysical and biochemical methods to examine the structural properties of PT S1. Our in vitro studies found that the isolated PT S1 subunit is a thermally unstable protein that can be degraded in a ubiquitin-independent fashion by the core 20S proteasome. The thermal denaturation of PT S1 was inhibited by its interaction with NAD, a donor molecule used by PT S1 for the ADP ribosylation of target G proteins. These observations support a model of intoxication in which toxin translocation, degradation, and activity are all influenced by the heat-labile nature of the isolated toxin A chain.

Pertussis toxin (PT)[1] is an AB-type protein toxin that consists of an enzymatic A moiety and a cell-binding B moiety (reviewed in refs *1* and *2*). PT A (the S1 subunit) activates certain Gα proteins by an ADP ribosylation reaction that utilizes NAD as a donor molecule. PT B is composed of an S2 subunit, an S3 subunit, two S4 subunits, and an S5 subunit. The oligomeric PT B complex forms a ringlike structure that is stable at temperatures of up to 60−70 °C (*3*). Noncovalent interactions position the catalytic S1 subunit within and on top of the B ring to form the PT holotoxin.

PT B binds to glycoproteins or glycolipids on the plasma membrane of a target cell (*4*−*6*). The surface-bound toxin then travels by vesicular transport to the Golgi apparatus and most likely to the endoplasmic reticulum (ER) as well (*7*−*12*). In the ER, ATP can bind to the central pore of the B oligomer and destabilize the holotoxin (*9*, *13*, *14*). Subsequent reduction of the PT S1 intramolecular disulfide bond may further destabilize the holotoxin and allow PT S1 to dissociate from PT B (*15*). The isolated S1 subunit can then cross the ER membrane and enter the cytosol to interact with its Gα targets (*16*, *17*).

The quality control system of ER-associated degradation (ERAD) may be involved with the ER-to-cytosol translocation of PT S1 (*10*). ERAD recognizes misfolded proteins (often identified by surface-exposed hydrophobic residues) in the ER and exports them to the cytosol for degradation by the ubiquitin−proteasome pathway (*18*). Export occurs through the Sec61p translocon, a gated pore in the ER membrane that allows bidirectional movement of partially or fully unfolded proteins between the ER and the cytosol (*19*). The C-terminal hydrophobic region of PT S1 is thought to trigger ERAD activity and stimulate translocation of PT S1 into the cytosol; proteasome-mediated degradation in the cytosol is presumably avoided because PT S1 has no lysine residues for ubiquitin attachment (*10*). Similar predictions have been made for cholera toxin (CT) and ricin, two other AB-type toxins that move from the cell surface to the ER and exploit ERAD for entry of the A chain into the cytosol (*10*, *20*).

Recent work has shown that the C-terminal region of PT S1 is not required for passage into the cytosol and has suggested that PT S1 may be degraded in the cytosol (*16*, *17*). Likewise, the CT A1 polypeptide does not require its C-terminal hydrophobic domain to move from the ER to the cytosol (*21*). Furthermore, CT A1 and ricin A chain are both degraded in the cytosol by ubiquitin-independent proteasomal mechanisms (*22*−*25*; K. Teter et al., unpublished experiments). These observations call for a modification to the current ERAD models of toxin translocation.

† This work was supported by National Institutes of Health Grant K22 AI054568 to K.T. and by start-up funds provided to K.T. from the University of Central Florida Department of Molecular Biology and Microbiology.

* To whom correspondence should be addressed. Telephone: (407) 882-2247. Fax: (407) 384-2062. E-mail: kteter@mail.ucf.edu.

‡ Department of Molecular Biology and Microbiology.

§ Biomolecular Science Center.

|| Present address: Biological Science Group, Corridor #3222, FD-III, Birla Institute of Technology and Sciences, Pilani 333 031 (RJ), India.

⊥ Student at Lake Highland Preparatory School, Orlando, FL.

[1] Abbreviations: β-ME, β-mercaptoethanol; CHAPS, 3-[(3-cholamidopropyl)dimethylammonio]-1-propanesulfonate; CT, cholera toxin; CD, circular dichroism; ER, endoplasmic reticulum; ERAD, endoplasmic reticulum-associated degradation; PT, pertussis toxin; SDS−PAGE, sodium dodecyl sulfate−polyacrylamide gel electrophoresis; T_m, transition temperature.

10.1021/bi061175+ CCC: $33.50
Published on Web 10/31/2006

We have proposed a revised model of toxin−ERAD interactions in which both toxin translocation and toxin degradation are linked to the heat-labile nature of the isolated toxin A moiety (*21*). With this model, thermal instability in the dissociated toxin A chain generates an unfolded conformational state at 37 °C that triggers ERAD activity and renders the cytosolic pool of toxin susceptible to degradation by the 20S proteasome (in contrast to the usual route of ubiquitin-dependent degradation by the 26S proteasome). Both CT A1 and ricin A chain are heat-labile proteins, and in vitro degradation of CT A1 by the 20S proteasome has been observed by our group (*26*; K. Teter et al., unpublished experiments). Here, structural studies and biochemical assays were used to examine the putative heat-labile nature of PT S1 and its possible degradation by the 20S proteasome. Analysis of the physical properties of the isolated PT A moiety supports our revised model of toxin−ERAD interactions. Furthermore, we provide a mechanism by which the PT S1 subunit can retain significant enzymatic activity in the cytosol despite its heat-labile state.

EXPERIMENTAL PROCEDURES

Materials. Chemicals and thermolysin were purchased from Sigma-Aldrich (St. Louis, MO). PT, PT S1, and PT B were from List Biological Laboratories, Inc. (Campbell, CA). ATP and the CT A1−A2 heterodimer were purchased from Calbiochem (La Jolla, CA). The purified 20S proteasome was from Boston Biochem (Cambridge, MA).

Circular Dichroism Measurements. Temperature-dependent unfolding of the PT S1 subunit was studied by circular dichroism (CD) experiments, using a J-810 spectrofluoropolarimeter equipped with a PFD-425S Peltier temperature controller (Jasco Corp., Tokyo, Japan). The protein concentration was 37.4 μg in 0.225 mL of 20 mM sodium phosphate buffer (pH 7.4) containing 150 mM NaCl and 10 mM β-mercaptoethanol (β-ME). Measurements were taken with a 4 mm optical path length rectangular quartz cuvette as the temperature increased stepwise from 18 to 50 °C. As shown in the thermal unfolding profiles, measurements were taken in 2 °C increments from 18 to 30 °C, 1 °C increments from 30 to 33 °C, 0.5 °C increments from 33 to 37 °C, a 1 °C increment from 37 to 38 °C, and 2 °C increments from 40 to 50 °C. Samples were allowed to equilibrate at each temperature for 4 min before readings were taken. CD spectra were recorded from 200 to 315 nm, which covers both near-UV and far-UV ranges and thus allowed us to detect thermal changes in both the tertiary and secondary structures of PT S1. The same sample was used for near-UV and far-UV measurements to eliminate possible errors resulting from sample-to-sample variability. In all cases, the spectral resolution was 1 nm. CD spectra were averaged from five scans. The observed ellipticity was converted to mean residue molar ellipticity, $[\theta]$, in units of degrees square centimeters per decimole using

$$[\theta] = \theta_{obs}/cn_{res}l \quad (1)$$

where θ_{obs} is the measured ellipticity in millidegrees, c is the molar concentration of the protein, n_{res} is the number of amino acid residues in the protein, and l is the optical path length in millimeters.

The temperature-dependent protein unfolding data were analyzed as described by Lavigne et al. (*27*) using the following equation:

$$X = f_L X_L + (1 - f_L)X_H \quad (2)$$

where X is the ellipticity measured at a given temperature, f_L is the fraction of amino acids representing the native conformation at low temperatures, and X_L and X_H are limiting values of X at low and high temperatures, respectively. The parameter f_L is given by

$$f_L = \exp(-\Delta G/RT)/[1 + \exp(-\Delta G/RT)] \quad (3)$$

where the temperature dependence of the free energy of unfolding (ΔG) is described by

$$\Delta G = \Delta H(1 - T/T_m) + \Delta C[T - T_m - T\ln(T/T_m)] \quad (4)$$

where T is the absolute temperature, T_m is the transition temperature, ΔH is the apparent enthalpy of unfolding, and ΔC is the heat capacity of unfolding.

Thermolysin Degradation Assay. For this, 6 μg of PT S1, 6 μg of the CT A1−A2 heterodimer, 12 μg of PT B, or 18 μg of PT was added to 0.12 mL of 20 mM sodium phosphate buffer (pH 7.0) containing 10 mM β-ME. Where indicated, 1 mM NAD, 1% CHAPS, or both 1 mM NAD and 1% CHAPS together were present in the sodium phosphate buffer; 20 μL sample aliquots were transferred to fresh microcentrifuge tubes and incubated at 4, 25, 33, 37, or 41 °C for 45 min. All samples were then shifted to 4 °C for 10 min. Thermolysin [prepared as a 10× stock in 50 mM $CaCl_2$ and 100 mM Hepes (pH 8.0)] was added to a final concentration of 0.04 mg/mL for a 45 min incubation at 4 °C. Digests were halted by the addition of 10 mM EDTA (final concentration) and SDS−PAGE sample buffer to the reaction mix. Toxin samples were visualized by SDS−PAGE and Coomassie staining. The NAD glycohydrolase activity of PT S1 at 37 °C is approximately 0.6 pmol min^{-1} (μg of toxin)$^{-1}$ (*28*). From this value, we estimate an inconsequential 0.14% of the NAD present in our assay buffer was hydrolyzed during the course of the experiment.

20S Proteasome Assay. For this, 5 μg of PT S1, 5 μg of the CT A1−A2 heterodimer, 10 μg of PT B, or 15 μg of PT was mixed with 100 nM purified 20S proteasome in 0.1 mL of assay buffer [100 mM KCl, 10 mM $MgCl_2$, 0.1 mM $CaCl_2$, 10 mM β-ME, 3 mM ATP, and 50 mM Hepes (pH 7.5)] and kept at 37 °C; 20 μL aliquots taken at the stated intervals were mixed with SDS−PAGE sample buffer visualized by SDS−PAGE with Coomassie staining.

RESULTS

Effect of Temperature on PT S1 Structure. The structure of PT has been determined by X-ray crystallography, which identified the S1 subunit as a 26 kDa protein with 28% α-helix content and 14% β-sheet content (*29*). To examine the thermal stability of PT S1, temperature-induced changes in the structure of PT S1 were monitored by near-UV and far-UV CD (Figure 1). The disruption of PT S1 tertiary structure was detected by a decrease in the magnitude of the near-UV CD signal from PT S1 aromatic side chains at ~280 nm (Figure 1A), while the loss of PT S1 secondary structure was detected by a decrease in the ellipticity in the

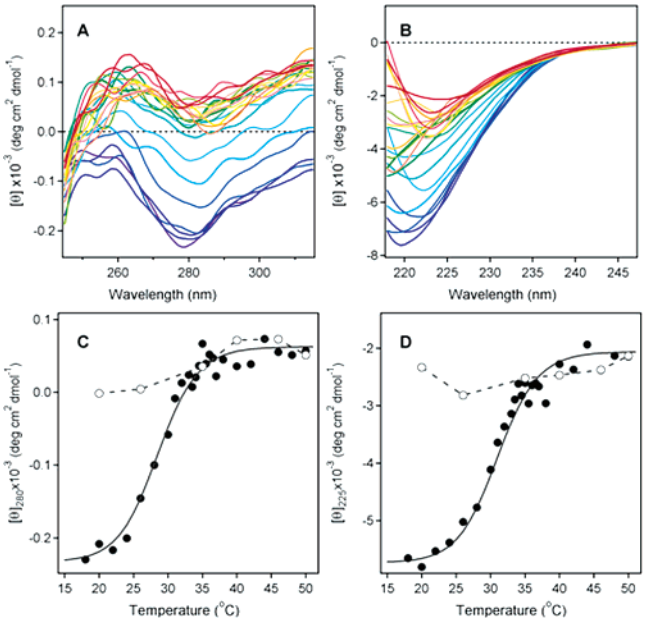

FIGURE 1: Temperature-induced unfolding of the PT S1 subunit. For panels A and B, 37.4 μg of PT S1 was dissolved in 0.225 mL of 20 mM sodium phosphate buffer (pH 7.4) containing 150 mM NaCl and 10 mM β-ME. Thermotropic conformational changes to the structure of PT S1 were then monitored by near-UV CD (A) and far-UV CD (B). Both measurements were conducted on the same sample with the use of a 4 mm optical path length rectangular quartz cuvette. Samples were equilibrated for 4 min at each temperature before the measurements were taken. CD spectra were recorded from 200 to 315 nm, which covers both the near-UV and far-UV range. The change in color from blue to red corresponds to a change in temperature from 18 to 50 °C, as shown in panels C and D. (C and D) Thermal unfolding profiles for the PT S1 tertiary structure (C) and PT S1 secondary structure (D) were derived from the data in panels A and B. The mean residue molar ellipticities at 280 nm (near-UV CD, tertiary structure) and 225 nm (far-UV CD, secondary structure) were plotted as a function of temperature. As described in Experimental Procedures, curves were simulated according to a two-state phase transition approach using the following best-fit parameters: heat capacities (ΔC) of 0.39 kcal mol^{-1} K^{-1} and ΔH values of 55.0 kcal/mol. The white circles represent measurements taken at the indicated temperatures during sample cooling from 50 to 18 °C.

far-UV region at ~225 nm (Figure 1B). The mean residue molar ellipticities at 280 and 225 nm then were plotted as a function of temperature to generate thermal unfolding profiles for the tertiary and secondary structures of PT S1. With these studies, we found thermotropic conformational changes occurred in a sigmodial manner for both the tertiary (Figure 1C) and secondary (Figure 1D) structures of PT S1. The transition temperature (T_m, the midpoint of transition) for the tertiary structure of PT S1 was 28.5 °C. The secondary structure of PT S1 exhibited a slightly higher T_m of 31.0 °C. Both values demonstrate that PT S1 is a heat-labile protein, with perturbed tertiary and secondary structures at the physiological temperature of 37 °C (see also Figure 2).

The thermal denaturation of PT S1 was irreversible (Figure 1C,D). After PT S1 had been heated to 50 °C, the toxin was cooled in stepwise increments to 18 °C. Measurements of the near- and far-UV CD spectra taken at various temperatures during sample cooling are represented by the empty circles in panels C and D. The data clearly indicate that PT S1 was unable to assume a native conformation following its temperature-induced unfolding at 50 °C.

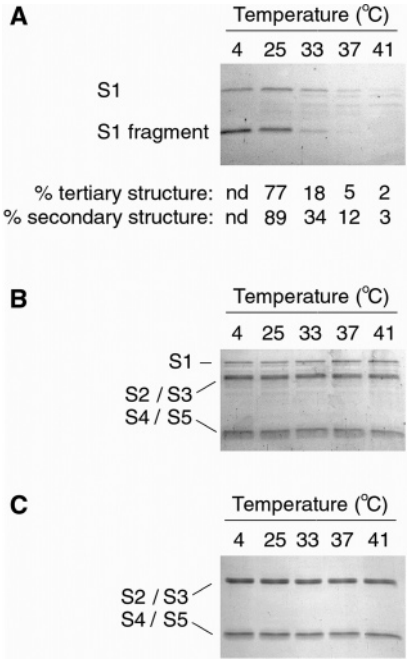

FIGURE 2: PT S1 protease sensitivity assay. (A) PT S1 was placed in 20 mM sodium phosphate buffer (pH 7.0) containing 10 mM β-ME. Toxin samples were incubated for 45 min at the indicated temperatures and then shifted to 4 °C for 10 min. Thermolysin was subsequently added for an additional 45 min at 4 °C. Samples were visualized by SDS−PAGE and Coomassie staining. The percentage of native tertiary and secondary structure remaining in PT S1 at the indicated temperatures was calculated from the thermal unfolding profiles presented in panels C and D of Figure 1, respectively. nd means not determined. (B and C) PT (B) and PT B (C) were processed as described above for PT S1. The subunits of PT are identified: S1 (26 kDa), S2 and S3 (~22 kDa each), and S4 and S5 (11−12 kDa).

Effect of Temperature, NAD, and CHAPS on PT S1 Protease Sensitivity. The temperature-dependent folding state of PT S1 was also monitored with a protease sensitivity assay (Figure 2). Samples of the purified and reduced PT S1 subunit were placed in 20 mM sodium phosphate buffer (pH 7.0) and incubated at 4, 25, 33, 37, or 41 °C for 45 min. All samples were then shifted to 4 °C and exposed to the metalloprotease thermolysin for an additional 45 min. Since all protease treatments were conducted at 4 °C, differential degradation of the PT S1 samples could result only from temperature-induced changes to the structure of PT S1. Thermolysin-treated samples were resolved by SDS−PAGE and visualized with Coomassie staining. Similar experiments were performed for PT and PT B.

As shown in Figure 2A, PT S1 samples preincubated at 37 or 41 °C were degraded by thermolysin. Substantial degradation of the PT S1 sample preincubated at 33 °C was also observed. PT S1 samples preincubated at 4 or 25 °C were nicked but not degraded by thermolysin. The ~18 kDa S1 fragment generated by thermolysin nicking of PT S1 most likely represents the N-terminal catalytic core of PT S1; similar N-terminal S1 fragments have also been detected in intoxicated cells (*30*, *31*) and after in vitro exposure of PT S1 to trypsin or chymotrypsin (*32*, *33*). For our assay, the S1 fragment did not appear without thermolysin treatment and was not generated from PT S1 samples co-incubated with EDTA and thermolysin (data not shown).

The extent of PT S1 degradation correlated well with its conformational state (Figure 2A, bottom panel); the protease-

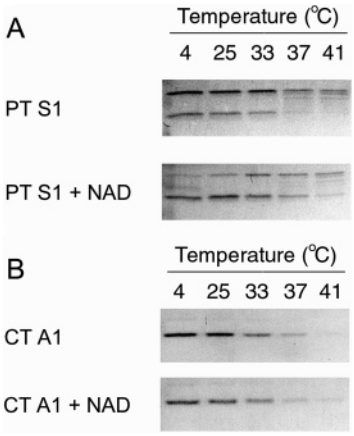

FIGURE 3: Effect of NAD on PT S1 protease sensitivity. PT S1 (A) and CT A1−A2 heterodimer (B) were placed in 20 mM sodium phosphate buffer (pH 7.0) containing 10 mM β-ME. NAD (1 mM) was present in the sodium phosphate buffer as indicated. Toxin samples were incubated at the stated temperatures for 45 min and then shifted to 4 °C for 10 min. Thermolysin was added for an additional 45 min at 4 °C. Samples were visualized by SDS−PAGE with Coomassie staining. In panel A, the top band is full-length PT S1 and the bottom band is the S1 fragment. In panel B, the 5 kDa CT A2 polypeptide was not visible after Coomassie staining.

resistant PT S1 sample that was incubated at 25 °C retained a significant amount of native tertiary and secondary structure, whereas the protease-sensitive PT S1 samples that were incubated at ≥37 °C retained little of the native toxin structure. When PT S1 was incubated at 33 °C, it retained an intermediate amount of native structure and was partially resistant to thermolysin-mediated degradation. These observations validated the use of a protease sensitivity assay to probe the folding state of PT S1 and demonstrated that PT S1 is in an unfolded, protease-sensitive conformation at 37 °C.

PT and PT B samples preincubated at 4, 25, 33, 37, and 41 °C were uniformly resistant to thermolysin-mediated degradation (Figure 2B,C). This demonstrated the specificity of thermolysin activity against the isolated PT S1 subunit and was consistent with the heat-stable properties of both PT and PT B (*3*, *34*). It also indicated that the association of PT S1 with PT B protected PT S1 from thermolysin-mediated degradation. Likewise, PT S1 is resistant to processing by trypsin and chymotrypsin when incorporated into the PT holotoxin (*32*, *33*). Thus, protease sensitivity (and thermal instability) in the PT S1 subunit is only apparent after it dissociates from PT B.

The heat-labile nature of the isolated PT S1 subunit suggests that the translocated, cytosolic pool of toxin would not function at 37 °C, yet intoxication occurs in vivo at 37 °C. In vitro, NAD glycohydrolase and ADP ribosylation assays have also documented PT S1 activity at 37 °C (*28*). Since both of these in vitro assays included NAD as a donor molecule, we hypothesized that an interaction between PT S1 and NAD could stabilize the structure of PT S1 and allow the toxin to function at 37 °C despite its heat-labile state. A similar relationship has been established for the heat-labile ricin A chain and its ribosome target (*26*).

To determine whether NAD has a stabilizing effect on the structure of PT S1, we performed our protease sensitivity assay on toxin samples that had been incubated with 1 mM NAD (Figure 3). In comparison to toxin samples incubated without NAD, PT S1 samples incubated with NAD exhibited

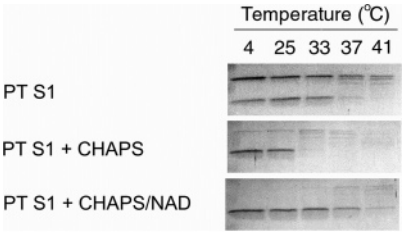

FIGURE 4: Effect of CHAPS on PT S1 protease sensitivity. PT S1 was placed in 20 mM sodium phosphate buffer (pH 7.0) containing 10 mM β-ME; 1% CHAPS or 1% CHAPS with 1 mM NAD was present in the sodium phosphate buffer as indicated. Toxin samples were incubated at the stated temperatures for 45 min and then shifted to 4 °C for 10 min. Thermolysin was added for an additional 45 min at 4 °C. Samples were visualized by SDS−PAGE with Coomassie staining. For the untreated PT S1 sample, the top band is full-length PT S1 and the bottom band is the S1 fragment. CHAPS-treated samples produced only the S1 fragment.

increased resistance to thermolysin-mediated degradation (Figure 3A). Co-incubation with NAD increased the susceptibility of PT S1 to thermolysin nicking, but in the presence of NAD, a substantial amount of this nicked S1 fragment (as well as the remaining full-length PT S1 polypeptide) was detected after incubations at 37 and 41 °C. Generation of the nicked PT S1 fragment indicated that thermolysin was active in the presence of NAD. Furthermore, NAD did not inhibit the thermolysin-mediated degradation of CT A1 (Figure 3B). Thus, NAD specifically inhibited the temperature-induced structural shift of PT S1 to a protease-sensitive conformation.

We also examined PT S1 protease sensitivity in the presence of CHAPS, a zwitterionic detergent that stimulates the in vitro enzymatic activity of PT and PT S1 (*28*, *35*, *36*). This stimulatory effect could conceivably result from CHAPS-mediated stabilization of the heat-labile PT S1 structure, yet CHAPS did not inhibit the temperature-induced structural shift of PT S1 to a protease-sensitive conformation (Figure 4). Instead, PT S1 proteolysis was slightly more efficient in the presence of CHAPS: toxin samples preincubated at 33 °C in the absence of CHAPS were partially degraded by thermolysin, whereas PT S1 samples preincubated at 33 °C in the presence of CHAPS were completely degraded by thermolysin. Furthermore, in the presence of CHAPS, the conversion of full-length PT S1 to the S1 fragment was complete. These observations indicated that CHAPS had some effect on the structural state of PT S1, but this effect did not inhibit the temperature-induced shift of PT S1 to a protease-sensitive conformation.

CHAPS and NAD both exerted structural effects on PT S1 when the two agents were mixed together with PT S1 (Figure 4). In the presence of CHAPS and NAD, there was a full conversion of PT S1 to the S1 fragment. However, the PT S1 fragment also exhibited substantial resistance to degradation by thermolysin. CHAPS therefore stimulated the conversion of PT S1 to the S1 fragment, but it did not override the NAD-induced structural shift of the S1 fragment to a protease-resistant conformation. As CHAPS is often used to stimulate the in vitro enzymatic activity of PT and PT S1 (*28*, *35*, *36*), our results allow a direct comparison between these published studies and the structural state of PT S1.

Degradation of PT S1 by the 20S Proteasome. The unfolded, protease-sensitive conformation of PT S1 at 37 °C could facilitate its degradation by the 20S proteasome.

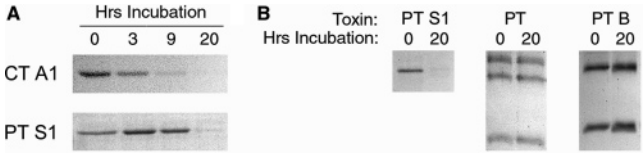

FIGURE 5: Degradation of PT S1 by the 20S proteasome. (A) Reduced PT S1 and the reduced CT A1−A2 heterodimer were incubated at 37 °C with the 20S proteasome. Toxin samples taken at the indicated time points were visualized by SDS−PAGE and Coomassie staining. (B) PT S1, PT, and PT B were incubated at 37 °C with the 20S proteasome under reducing conditions. Toxin samples taken after incubation for 0 or 20 h were visualized by SDS−PAGE and Coomassie staining.

This barrel-shaped structure comprises the catalytic core of the 26S proteasome, which is generated by the attachment of 19S regulatory particles to one or both ends of the 20S proteasome. Most proteasomal substrates are degraded in a ubiquitin-dependent process by the 26S proteasome, but a few proteins are instead degraded by a ubiquitin-independent mechanism involving only the core 20S proteasome (*37*, *38*). Proteins degraded by the 20S proteasome must be unfolded to pass through the central catalytic pore of the proteasome, and this unfolding event represents the rate-limiting step in proteolysis by the 20S proteasome (*38*, *39*). The unfolded structural state of PT S1 at 37 °C would therefore make it a suitable substrate for degradation by the 20S proteasome.

To monitor toxin degradation by the 20S proteasome, we incubated reduced CT A1 or reduced PT S1 with the 20S proteasome at 37 °C for 0, 3, 9, and 20 h (Figure 5A). CT A1 is a substrate for the 20S proteasome (K. Teter et al., unpublished experiments), and it was used here as a positive control for proteasomal activity. Toxin samples were resolved by SDS−PAGE and visualized with Coomassie staining. Both CT A1 and PT S1 were degraded by the 20S proteasome, even though ubiquitin and the ubiquitin conjugation machinery were absent from our assay conditions. CT A1 was degraded more efficiently than PT S1; whereas significant degradation of CT A1 was observed after incubation for 3 h, incubation for more than 9 h was required for detection of the degradation of PT S1. This slow rate of in vitro proteolysis is common for 20S proteasome substrates (*40*−*42*) and may be accelerated in vivo by proteasome accessory factors such as hsp90 (*43*).

To further evaluate the specificity of our proteasome assay, we incubated PT S1, PT, or PT B with the 20S proteasome for 20 h at 37 °C (Figure 5B). The isolated PT S1 subunit was effectively degraded by the 20S proteasome. However, PT S1 degradation did not occur when the A moiety was incorporated into the PT holotoxin. This again indicated that the structural arrangement of the holotoxin prevented PT S1 from assuming a protease-sensitive (i.e., unfolded) conformation. It also demonstrated that indiscriminate proteasomal degradation was not responsible for proteolysis of the isolated PT S1 subunit. The specificity of proteasomal activity was further confirmed by the stability of the PT B oligomer in the presence of the 20S proteasome.

As the core 20S proteasome can only degrade unfolded substrates, the stabilizing effect of NAD on PT S1 structure could protect the toxin from ubiquitin-independent degradation by the 20S proteasome. However, addition of 1 mM NAD to the assay buffer did not prevent degradation of PT S1 by the 20S proteasome (data not shown). Thus, NAD-induced stabilization of the PT S1 catalytic core (see Figures 3 and 4) is not sufficient to protect the PT S1 polypeptide from processing by the 20S proteasome.

DISCUSSION

Contrary to current models of ERAD-mediated toxin translocation, the C-terminal region of PT S1 is not required for the toxin to pass into the cytosol (*16*, *17*). PT S1 may also be degraded in the cytosol (*16*). On the basis of these observations and our recent work with the CT A1 polypeptide (*21*), we hypothesized ER-translocating toxins such as PT contain thermally unstable A subunits that are susceptible to degradation by the 20S proteasome. The work presented here provides direct experimental evidence that supports this hypothesis and suggests a new model for toxin−ERAD interactions.

The tertiary structure of PT S1 unfolds with a T_m of 28.5 °C, and the secondary structure of PT S1 becomes disordered with a T_m of 31.0 °C. Thus, the isolated and reduced PT S1 subunit is structurally unstable at physiological temperature. PT S1 is also in a protease-sensitive state at 37 °C. These observations stand in marked contrast to the heat-stable and protease-resistant properties of both PT and PT B, which only unfold at temperatures greater than 60 °C (*3*, *34*). The structure of the PT holotoxin thus maintains PT S1 in a stable conformation until the toxin is exposed to an environment (i.e., the ER lumen) that allows PT S1 to dissociate from PT B. A similar structural relationship exists for the subunits of CT (*44*, *45*) (K. Teter et al., unpublished experiments), so the stabilizing effect of A−B interactions on the heat-labile structure of the toxin A moiety may be a general phenomenon for AB-type, ER-translocating toxins. The proposed role of PT B as a scaffold to stabilize the heat-labile structure of PT S1 complements the apparent role of PT B as a targeting vehicle for delivery of PT S1 to the ER (*12*, *16*, *17*).

Dissociation of PT S1 from PT B in the ER of an intoxicated cell would apparently result in the spontaneous unfolding of PT S1. This unfolding event, which is likely required for passage through the Sec61p translocon, could stimulate the ERAD-mediated translocation of PT S1 into the cytosol. By this model, the unfolded conformation of PT S1 at 37 °C allows it to masquerade as a misfolded protein. ERAD-mediated toxin translocation was originally thought to depend upon a hydrophobic domain in the C-terminal region of the toxin A chain (*10*), but neither CT A1 nor PT S1 requires their C-terminal domains for passage into the cytosol (*16*, *17*, *21*). Our structural studies provide an alternative trigger for the ERAD mechanism that is based upon the heat-labile state of the isolated toxin A chain. This property results in chaperone-independent unfolding of PT S1 at 37 °C, although in vivo unfolding of the toxin A chain may be initiated or aided by ER-localized chaperones and oxidoreductases.

The translocated and cytosolic pool of PT S1 might be stabilized by its association with NAD, the donor molecule for the ADP ribosylation reaction that modifies the G protein targets of PT. We could not obtain a thermal unfolding profile for PT S1 in the presence of NAD because of the interfering signal produced by NAD in CD measurements. Structural measurements with fluorescence spectroscopy were also

hampered by the quenching effect NAD has on PT S1 fluorescence (*46*, *47*). However, a protease sensitivity assay demonstrated the inhibitory effect of NAD on the temperature-induced structural shift of PT S1 to a protease-sensitive (i.e., unfolded) conformation. Although full-length PT S1 was still susceptible to thermolysin nicking in the presence of NAD, the resulting S1 fragment (which represents the catalytic core of PT S1) exhibited increased stability in the presence of NAD. This result was consistent with the reported ability of NAD to protect the enzymatic activity of reduced PT S1 during incubations at 30 °C (*48*). Collectively, these observations provide an explanation for how PT S1 can regain an active conformation (via NAD binding) after entering the cytosol in an unfolded state.

The cellular concentration of NAD is estimated to be 3 mM (*49*, *50*). Up to 80% of cellular NAD is found in the cytosol; the bulk of the remaining NAD is located in the mitochondria (*49*). As the ER does not contain a substantial pool of NAD, the thermal unfolding of PT S1 can occur at this site without interference from NAD. Furthermore, the cytosolic concentration of NAD is well above the K_d of 25 μM for NAD with PT S1 (*47*). It is therefore feasible for the cytosolic pool of NAD to readily interact with, and stabilize, the translocated PT S1 subunit. The subcellular distribution of NAD, which is absent from the ER and present in the cytosol at millimolar levels, thus conforms to our model of PT S1 translocation.

CT A1 and other toxins also use NAD as a donor molecule for the ADP ribosylation of target substrates (*1*). However, as assessed with our protease sensitivity assay, NAD did not inhibit the thermal denaturation of CT A1. This indicated that (i) NAD does not directly inhibit thermolysin activity and (ii) the stabilizing effect of NAD on PT S1 is not a common phenomenon for all ADP-ribosylating toxins. In the case of CT, an interaction with ADP ribosylation factors is likely to stabilize and/or renature the heat-labile CT A1 subunit (*51*).

CHAPS, a zwitterionic detergent that stimulates PT and PT S1 activity in vitro (*28*, *35*, *36*), also affected the structural state of PT S1. It did not, however, inhibit the thermal denaturation of PT S1: nearly identical near- and far-UV CD thermal unfolding profiles were obtained for PT S1 samples incubated in either the presence or absence of 0.5% CHAPS (data not shown). Instead, CHAPS induced a structural shift that stimulated the thermolysin-mediated conversion of PT S1 to the S1 fragment. This structural shift may enhance the enzymatic activity of PT S1, as CHAPS provides a 2-fold stimulation of PT S1 NAD glycohydrolase activity at 37 °C and a greater level of stimulation at 30 °C (*28*, *35*). Interestingly, the S1 fragment generated by exposure to CHAPS and thermolysin was held in a protease-resistant conformation when NAD was also present in the sample buffer. This again emphasized the stabilizing effect of NAD on the catalytic core of PT S1.

PT S1 may be degraded in the eukaryotic cytosol despite the absence of lysine residues for ubiquitin attachment (*16*). A ubiquitin-independent mechanism for toxin degradation could involve processing by the core 20S proteasome, which acts upon CT A1 and other unfolded or partially unfolded proteins (*37*, *38*). The unfolded, protease-sensitive state of PT S1 at 37 °C would therefore place it in the proper conformation for degradation by the 20S proteasome. This prediction was confirmed with an in vitro assay demonstrating the susceptibility of PT S1 to ubiquitin-independent degradation by the core 20S proteasome. Thus, the heat-labile nature of PT S1 could possibly influence both its translocation into the cytosol and its degradation in the cytosol.

The 20S proteasome degraded CT A1 more rapidly than PT S1, even though CT A1 retains more of its native structure at 37 °C than PT S1. Thus, the efficiency of substrate processing by the 20S proteasome is not always directly proportional to the extent of substrate unfolding. Additional factors such as substrate recognition/binding and structural constraints on substrate passage into the central pore of the proteasome are likely to affect the efficiency of substrate processing by the 20S proteasome as well. The differential processing of CT A1 and PT S1 by the 20S proteasome suggests that these toxins could serve as useful probes in future work aimed at dissecting the mechanics of degradation by the core 20S proteasome.

The in vitro studies of this work have demonstrated that the isolated and reduced PT S1 subunit is a thermally unstable protein susceptible to degradation by the 20S proteasome. This provides experimental evidence for a revised model of toxin−ERAD interactions in which both toxin translocation and toxin degradation are linked to an inherent physical property (i.e., thermal instability) of the toxin A moiety.

REFERENCES

1. Krueger, K. M., and Barbieri, J. T. (1995) The family of bacterial ADP-ribosylating exotoxins, *Clin. Microbiol. Rev. 8*, 34−47.
2. Kaslow, H. R., and Burns, D. L. (1992) Pertussis toxin and target eukaryotic cells: Binding, entry, and activation, *FASEB J. 6*, 2684−2690.
3. Yang, J., Mou, J., and Shao, Z. (1994) Structure and stability of pertussis toxin studied by in situ atomic force microscopy, *FEBS Lett. 338*, 89−92.
4. Brennan, M. J., David, J. L., Kenimer, J. G., and Manclark, C. R. (1988) Lectin-like binding of pertussis toxin to a 165-kilodalton Chinese hamster ovary cell glycoprotein, *J. Biol. Chem. 263*, 4895−4899.
5. Hausman, S. Z., and Burns, D. L. (1993) Binding of pertussis toxin to lipid vesicles containing glycolipids, *Infect. Immun. 61*, 335−337.
6. Witvliet, M. H., Burns, D. L., Brennan, M. J., Poolman, J. T., and Manclark, C. R. (1989) Binding of pertussis toxin to eucaryotic cells and glycoproteins, *Infect. Immun. 57*, 3324−3330.
7. Xu, Y., and Barbieri, J. T. (1995) Pertussis toxin-mediated ADP-ribosylation of target proteins in Chinese hamster ovary cells involves a vesicle trafficking mechanism, *Infect. Immun. 63*, 825−832.
8. Xu, Y., and Barbieri, J. T. (1996) Pertussis toxin-catalyzed ADP-ribosylation of Gi-2 and Gi-3 in CHO cells is modulated by inhibitors of intracellular trafficking, *Infect. Immun. 64*, 593−599.
9. Hazes, B., Boodhoo, A., Cockle, S. A., and Read, R. J. (1996) Crystal structure of the pertussis toxin-ATP complex: A molecular sensor, *J. Mol. Biol. 258*, 661−671.
10. Hazes, B., and Read, R. J. (1997) Accumulating evidence suggests that several AB-toxins subvert the endoplasmic reticulum-associated protein degradation pathway to enter target cells, *Biochemistry 36*, 11051−11054.
11. el Baya, A., Linnemann, R., von Olleschik-Elbheim, L., Robenek, H., and Schmidt, M. A. (1997) Endocytosis and retrograde transport of pertussis toxin to the Golgi complex as a prerequisite for cellular intoxication, *Eur. J. Cell Biol. 73*, 40−48.
12. Carbonetti, N. H., Irish, T. J., Chen, C. H., O'Connell, C. B., Hadley, G. A., McNamara, U., Tuskan, R. G., and Lewis, G. K. (1999) Intracellular delivery of a cytolytic T-lymphocyte epitope peptide by pertussis toxin to major histocompatibility complex

class I without involvement of the cytosolic class I antigen processing pathway, *Infect. Immun. 67*, 602−607.
13. Burns, D. L., and Manclark, C. R. (1986) Adenine nucleotides promote dissociation of pertussis toxin subunits, *J. Biol. Chem. 261*, 4324−4327.
14. Krueger, K. M., and Barbieri, J. T. (1993) Molecular characterization of the in vitro activation of pertussis toxin by ATP, *J. Biol. Chem. 268*, 12570−12578.
15. Burns, D. L., and Manclark, C. R. (1989) Role of cysteine 41 of the A subunit of pertussis toxin, *J. Biol. Chem. 264*, 564−568.
16. Castro, M. G., McNamara, U., and Carbonetti, N. H. (2001) Expression, activity and cytotoxicity of pertussis toxin S1 subunit in transfected mammalian cells, *Cell. Microbiol. 3*, 45−54.
17. Veithen, A., Raze, D., and Locht, C. (2000) Intracellular trafficking and membrane translocation of pertussis toxin into host cells, *Int. J. Med. Microbiol. 290*, 409−413.
18. McCracken, A. A., and Brodsky, J. L. (2003) Evolving questions and paradigm shifts in endoplasmic-reticulum-associated degradation (ERAD), *BioEssays 25*, 868−877.
19. Romisch, K. (1999) Surfing the Sec61 channel: Bidirectional protein translocation across the ER membrane, *J. Cell Sci. 112* (Part 23), 4185−4191.
20. Lord, J. M., and Roberts, L. M. (1998) Toxin entry: Retrograde transport through the secretory pathway, *J. Cell Biol. 140*, 733−736.
21. Teter, K., Jobling, M. G., Stentz, D., and Holmes, R. K. (2006) The Cholera Toxin A13 Subdomain Is Essential for Interaction with ADP-Ribosylation Factor 6 and Full Toxic Activity but Is Not Required for Translocation from the Endoplasmic Recticulum to the Cytosol, *Infect. Immun. 74*, 2259−2267.
22. Simpson, J. C., Roberts, L. M., Romisch, K., Davey, J., Wolf, D. H., and Lord, J. M. (1999) Ricin A chain utilises the endoplasmic reticulum-associated protein degradation pathway to enter the cytosol of yeast, *FEBS Lett. 459*, 80−84.
23. Deeks, E. D., Cook, J. P., Day, P. J., Smith, D. C., Roberts, L. M., and Lord, J. M. (2002) The low lysine content of ricin A chain reduces the risk of proteolytic degradation after translocation from the endoplasmic reticulum to the cytosol, *Biochemistry 41*, 3405−3413.
24. Di Cola, A., Frigerio, L., Lord, J. M., Ceriotti, A., and Roberts, L. M. (2001) Ricin A chain without its partner B chain is degraded after retrotranslocation from the endoplasmic reticulum to the cytosol in plant cells, *Proc. Natl. Acad. Sci. U.S.A. 98*, 14726−14731.
25. Teter, K., Allyn, R. L., Jobling, M. G., and Holmes, R. K. (2002) Transfer of the cholera toxin A1 polypeptide from the endoplasmic reticulum to the cytosol is a rapid process facilitated by the endoplasmic reticulum-associated degradation pathway, *Infect. Immun. 70*, 6166−6171.
26. Argent, R. H., Parrott, A. M., Day, P. J., Roberts, L. M., Stockley, P. G., Lord, J. M., and Radford, S. E. (2000) Ribosome-mediated folding of partially unfolded ricin A-chain, *J. Biol. Chem. 275*, 9263−9269.
27. Lavigne, P., Crump, M. P., Gagne, S. M., Hodges, R. S., Kay, C. M., and Sykes, B. D. (1998) Insights into the mechanism of heterodimerization from the ^{1}H-NMR solution structure of the c-Myc-Max heterodimeric leucine zipper, *J. Mol. Biol. 281*, 165−181.
28. Murayama, T., Hewlett, E. L., Maloney, N. J., Justice, J. M., and Moss, J. (1994) Effect of temperature and host factors on the activities of pertussis toxin and *Bordetella* adenylate cyclase, *Biochemistry 33*, 15293−15297.
29. Stein, P. E., Boodhoo, A., Armstrong, G. D., Cockle, S. A., Klein, M. H., and Read, R. J. (1994) The crystal structure of pertussis toxin, *Structure 2*, 45−57.
30. Finck-Barbancon, V., and Barbieri, J. T. (1996) Preferential processing of the S1 subunit of pertussis toxin that is bound to eukaryotic cells, *Mol. Microbiol. 22*, 87−95.
31. Carbonetti, N. H., Mays, R. M., Artamonova, G. V., Plaut, R. D., and Worthington, Z. E. (2005) Proteolytic cleavage of pertussis toxin S1 subunit is not essential for its activity in mammalian cells, *BMC Microbiol. 5*, 7.
32. Burns, D. L., Hausman, S. Z., Lindner, W., Robey, F. A., and Manclark, C. R. (1987) Structural characterization of pertussis toxin A subunit, *J. Biol. Chem. 262*, 17677−17682.
33. Krueger, K. M., Mende-Mueller, L. M., and Barbieri, J. T. (1991) Protease treatment of pertussis toxin identifies the preferential cleavage of the S1 subunit, *J. Biol. Chem. 266*, 8122−8128.
34. Krell, T., Greco, F., Nicolai, M. C., Dubayle, J., Renauld-Mongenie, G., Poisson, N., and Bernard, I. (2003) The use of microcalorimetry to characterize tetanus neurotoxin, pertussis toxin and filamentous haemagglutinin, *Biotechnol. Appl. Biochem. 38*, 241−251.
35. Moss, J., Stanley, S. J., Watkins, P. A., Burns, D. L., Manclark, C. R., Kaslow, H. R., and Hewlett, E. L. (1986) Stimulation of the thiol-dependent ADP-ribosyltransferase and NAD glycohydrolase activities of *Bordetella pertussis* toxin by adenine nucleotides, phospholipids, and detergents, *Biochemistry 25*, 2720−2725.
36. Kaslow, H. R., Lim, L. K., Moss, J., and Lesikar, D. D. (1987) Structure-activity analysis of the activation of pertussis toxin, *Biochemistry 26*, 123−127.
37. Orlowski, M., and Wilk, S. (2003) Ubiquitin-independent proteolytic functions of the proteasome, *Arch. Biochem. Biophys. 415*, 1−5.
38. Shringarpure, R., Grune, T., and Davies, K. J. (2001) Protein oxidation and 20S proteasome-dependent proteolysis in mammalian cells, *Cell. Mol. Life Sci. 58*, 1442−1450.
39. Ferrington, D. A., Sun, H., Murray, K. K., Costa, J., Williams, T. D., Bigelow, D. J., and Squier, T. C. (2001) Selective degradation of oxidized calmodulin by the 20 S proteasome, *J. Biol. Chem. 276*, 937−943.
40. Pacifici, R. E., Kono, Y., and Davies, K. J. (1993) Hydrophobicity as the signal for selective degradation of hydroxyl radical-modified hemoglobin by the multicatalytic proteinase complex, proteasome, *J. Biol. Chem. 268*, 15405−15411.
41. Reinheckel, T., Sitte, N., Ullrich, O., Kuckelkorn, U., Davies, K. J., and Grune, T. (1998) Comparative resistance of the 20S and 26S proteasome to oxidative stress, *Biochem. J. 335* (Part 3), 637−642.
42. Tanaka, K., Waxman, L., and Goldberg, A. L. (1983) ATP serves two distinct roles in protein degradation in reticulocytes, one requiring and one independent of ubiquitin, *J. Cell Biol. 96*, 1580−1585.
43. Whittier, J. E., Xiong, Y., Rechsteiner, M. C., and Squier, T. C. (2004) Hsp90 enhances degradation of oxidized calmodulin by the 20 S proteasome, *J. Biol. Chem. 279*, 46135−46142.
44. Surewicz, W. K., Leddy, J. J., and Mantsch, H. H. (1990) Structure, stability, and receptor interaction of cholera toxin as studied by Fourier-transform infrared spectroscopy, *Biochemistry 29*, 8106−1811.
45. Goins, B., and Freire, E. (1988) Thermal stability and intersubunit interactions of cholera toxin in solution and in association with its cell-surface receptor ganglioside GM1, *Biochemistry 27*, 2046−5202.
46. Antoine, R., Tallett, A., van Heyningen, S., and Locht, C. (1993) Evidence for a catalytic role of glutamic acid 129 in the NAD-glycohydrolase activity of the pertussis toxin S1 subunit, *J. Biol. Chem. 268*, 24149−24155.
47. Lobban, M. D., Irons, L. I., and van Heyningen, S. (1991) Binding of NAD^+ to pertussis toxin, *Biochim. Biophys. Acta 1078*, 155−160.
48. Kaslow, H. R., Schlotterbeck, J. D., Mar, V. L., and Burnette, W. N. (1989) Alkylation of cysteine 41, but not cysteine 200, decreases the ADP-ribosyltransferase activity of the S1 subunit of pertussis toxin, *J. Biol. Chem. 264*, 6386−6390.
49. Devin, A., Nogueira, V., Leverve, X., Guerin, B., and Rigoulet, M. (2001) Allosteric activation of pyruvate kinase via NAD^+ in rat liver cells, *Eur. J. Biochem. 268*, 3943−3949.
50. Zocchi, E., Usai, C., Guida, L., Franco, L., Bruzzone, S., Passalacqua, M., and De Flora, A. (1999) Ligand-induced internalization of CD38 results in intracellular Ca^{2+} mobilization: Role of NAD^+ transport across cell membranes, *FASEB J. 13*, 273−283.
51. Murayama, T., Tsai, S. C., Adamik, R., Moss, J., and Vaughan, M. (1993) Effects of temperature on ADP-ribosylation factor stimulation of cholera toxin activity, *Biochemistry 32*, 561−566.

BI061175+